Published in: Drying Technology (2003), vol.21, iss.8, pp. 1507-1526
Status: Postprint (Author's version)

Multiscale Texture Characterization of Wastewater Sludges Dried in a Convective Rig

A. Léonard, S. Blacher, R. Pirard, P. Marchot, J. P. Pirard, and M. Crine

Laboratory of Chemical Engineering, Department of Applied Chemistry, University of Liège, Liège, Belgium

Abstract

Secondary sludges from two different wastewater treatment plants are conditioned and dewatered in the same way before drying in a lab-scale convective rig at the same operating conditions. Several techniques are used to characterize the texture of the dried materials over a wide range of scales from nm up to mm. Texture and porosity of the dried products are studied by SEM imaging, nitrogen absorption isotherms ($0.5 < d_p < 50$nm), mercury porosimetry ($7.5\text{nm} < d_p < 150\mu\text{m}$) and X-ray microtomography (spatial resolution = 41 µm). The image analysis of cross-sections reconstructed by microtomography also allows following shrinkage and textural evolution during drying.

Keywords: Wastewater sludges; Convective drying; SEM; N_2 isotherms; Hg porosimetry; X-ray microtomography.

INTRODUCTION

The directive of the Council of European Communities concerning urban wastewater treatment[1] will cause the multiplication of the number of wastewater treatment plants across Europe, and in turn will lead to a dramatic increase in the production of sludges. This production is expected to double in the EU during the next 10 years. At the same time, the directive on waste landfill plans the progressive reduction of sludge disposal in dump sites.[2] Two major issues will remain for sludge disposal: incineration and landspreading. In both cases, a thermal drying step is often needed after mechanical dewatering by centrifugation or nitration. Drying can reduce the water content below 5% DS, which offers several advantages. The reduction of mass and volume leads to a cost reduction in transport, handling, and storage and to an increase in concentration of fertilizer matter. Moreover, the dried sludge is stabilized and is free of pathogen germs due to the high temperature treatment. Finally, the removal of water to such a low level drastically increases the lower calorific value, transforming the sludge into an acceptable combustible.

Despite obvious economic, industrial, and environmental interests, rather few studies have been devoted to wastewater sludge drying till lately. Research in this field is however progressively growing, as indicated by recent publications.[3, 11] One reason for this lack of literature may be the complexity of activated sludges, which are heterogeneous mixtures of microorganisms, mineral particles, colloids, organic polymers, and cations,[12] whose composition varies considerably depending on sample origin and sampling date.[13] Their drying behavior as well as their final properties may strongly vary from one sludge sample to another. Actually, there are probably as many sludges as there are different WWTPs. There is a need for a comprehensive textural characterization covering a wide range of scales from nm to mm. This textural characterization may give some interesting data to better elucidate drying mechanisms and to identify final sludge properties adapted to landspreading or burning. The aim of this article is to apply some independent characterization techniques to illustrate the differences that may exist between sludge samples from two distinct WWTPs. Laser beam diffraction granulometer allows determining granulometric distribution of sludges before dewatering. Texture and porosity of the dried product are studied by scanning electronic microscopy imaging (SEM), nitrogen absorption isotherms ($0.5 < d_p < 50$nm), mercury porosimetry ($7.5\text{ nm} < d_p < 150\ \mu\text{m}$) and X-ray microtomography (spatial resolution = 41 µm). Image analysis of cross-sections obtained by microtomography also allows following shrinkage and textural evolution during drying.

Published in: Drying Technology (2003), vol.21, iss.8, pp. 1507-1526
Status: Postprint (Author's version)

MATERIALS AND METHODS

Sludge Samples

Sludge samples are collected in two domestic WWTPs after secondary settling and thickening. Sludge samples of 400 mL in 1 L beaker are flocculated in a bench scale jar-test by adding 0.006 kg/kg DS of a cationic polyelectrolyte (Zetag 7587 from Ciba). Samples are mixed at 120 rpm for l min. Agitation is then slowed down to 40 rpm for 3 min. Dewatering is realized in a normalized filtration-expression cell[14] under a differential pressure of 300 kPa. Filtration is stopped after 1 h. The recovered cake is extruded through a circular die of 12 mm diameter, producing cylindrical extrudates similar to those used in several industrial belt dryers. Extrudates are cut at a height of 15 mm, yielding samples with volume and mass of approximately 1.7 cm^3 and 2g, respectively.

The different WWTPs are called A and B. They differ by their capacity, i.e., their number of equivalent inhabitants (see Table 1). Another essential difference is the type of treatment. WWTP A has no nutrient removal stage, whereas WWTP B has an intermittent nitrification-denitrification stage. Table 1 also shows some characteristics of the two types of sludges, before and after mechanical dewatering. Dry solid content (DS) is measured by desiccating sludge sample at 105°C during 24 h and volatile solids are determined by calcinating dried sludge at 550°C during 2h. The sludge mean particle sizes (size range between 1.2 and 600 µm) are measured with a Malvern Mastersizer laser beam diffraction granulometer. They are approximately the same for sludge A and B. Before dewatering, the total solid content of sludge B is smaller than in sludge A: sludge B is more diluted. An opposite situation prevails after mechanical dewatering, sludge B reaching a higher solid content. These different dewatering performances should be due to the different nature of both sludges. Unlike usually, in our case, the more mineral sludge is not the easier to dewater.

Table 1. *Characteristics of the two types of sludges, before and after mechanical dewatering.*

	WWTP A	WWTP B
Number of equivalent inhabitants	9,000	27,000
Sludge mean particle size (µm)	55 ± 47	62 ± 44
Sludge total solid content before dewatering (%)	4.67 ± 0.01	2.99 ± 0.02
Sludge total solid content after dewatering (%)	14.2 ± 0.3	19.3 ± 0.5
Sludge volatile solids (% of DS)	44.8 ± 0.5	63.5 ± 1.2

Convective Micro-Dryer

The microdryer used in this study is a classical convective rig controlled in relative humidity, temperature, and air velocity. It has already been described in detail in a previous article.[10] Drying conditions reported in this article correspond to air at ambient humidity (~0.007 kg water/kg dry air) and at a temperature of 160°C. The superficial air velocity is kept at 3 m/s.

Characterization Devices

SEM (Scanning Electron Microscope)

Small fragments of dried sludges are mounted on an aluminum stub with a carbon adhesive and then coated with platinum (120 s, Argon atmosphere) before observation with a "Jeol JSM-840A SEM" (Jeol, USA) operating at an accelerating voltage of 20 kV.

X-Ray Microtomograph and Image Analysis

Microtomography is used to monitor the evolution of the volume, the external surface and the texture of the sludge samples. Indeed, sludges are soft, pasty materials that undergo large deformations and develop some cracks during drying. The X-ray tomographic device used in this study is a "Skyscan-1074 X-ray scanner" (Skyscan, Belgium). The X-ray source operates at 40 kV and 1 mA. The detector is a 2D, 768 x 576 pixels, 8-bit X-ray camera with a spatial resolution of 41 µm. The sample can be either rotated in a horizontal plane or moved vertically in order to get scans at different vertical positions. The minimum vertical distance between two scans

equals 41 µm. Once the sample is placed in the microtomograph, four projections are recorded in order to determine the height of the sample. A zone covering approximately a height of 10 mm is selected for tomographic investigation: around 20 transversal sections separated by 0.41 mm are then recorded. This operation is repeated several times during one drying run. 2D cross-sections and projections are processed and analyzed using basic tools of mathematical morphology and signal processing, [15,16] as explained elsewhere.[17] Appropriated programs are implemented in Matlab software, with image analysis toolbox version 3.1 from Matworks.

Nitrogen Adsorption Isotherms

Nitrogen adsorption isotherms measurements are performed at 77 K on a "Micrometrics ASAP 2010M" (Micrometrics Inst. Co., USA) and on a "Fisons Sorptomatic 1990" (Fisons Instruments, UK). Each isotherm point is acquired when the pressure variation, within a fixed time, is lower than a fixed pressure deviation.

Mercury Porosimetry

Mercury porosimetry measurements are performed using a porosi-meter Carlo Erba 2000 (CE Instruments, formerly Carlo Erba, UK). They are made between 0.01 and 200 MPa. The measurement of the largest pore sizes is carried out under atmospheric pressure using a manual porosimeter. The Washburn equation (Eq. (1))[18] is used to calculate the pore diameter, d_p, in relation to the external pressure, P, applied to force mercury, a nonwetting liquid, into the pores, σ is the surface tension of mercury (0.48 Nm^{-1}) and θ is the contact angle of mercury onto the pore walls (140°). The range of pressure investigated allows us to study pores with diameters between 7.5 nm and 150 µm. Visual observations of the recovered samples after measurement indicate that sludge is intruded without any collapse.

$$P = -\frac{4\sigma\cos\theta}{d_p} \qquad (1)$$

RESULTS

Two extrudate samples of each sludge are used for the drying experiments: the first one is dried without any interruption, while the second one is removed several times from the dryer for tomographic investigation. For the first extrudate sample, only tomographic images of first (wetted) and last (completely dried) states are recorded. Initial and final mass of sludges A and B as well as their water content (on a dry basis) are listed in Table 2.

Although extrudates 1 and 2 are sampled in the same filtration cake, their water contents slightly differ, as it can be seen in Table 2. This can be explained either by vertical moisture gradient within the cake, resulting from pressure profiles that develop during filtration[19] or by the heterogeneity of the investigated product.

SEM Images

SEM micrographs of the external surface of dried samples of sludges A and B at magnifications of 50x and 5000x are shown in Figs. 1a-d. At higher magnifications, image focusing is hard to achieve. At high magnification, the structure of sludge A (Fig. 1c) seems denser and more compact than that of sludge B (Fig. 1d). The structure of sludge A seems made of a complex arrangement of aggregate-like elements, while sludge B presents a kind of smooth branched-network. Observations at low resolution allow examining the whole structure. The surface of sample A (Fig. la) seems rather smooth and crossed by large cracks. The surface of sample B (Fig. lb) presents a more open and complex structure constituted by a hierarchy of pores of various sizes and forms. In other words, sludge B exhibits a rougher surface than sludge A does. Such differences are difficult to explain. They may result from differences in the type of biological process used in WWTPs A and B (see materials and methods).

Nitrogen Adsorption-Desorption

N_2 adsorption-desorption measurements allow scanning pore diameters between 0.5 and 50 nm. Figure 2 shows the N_2 adsorption-desorption isotherms obtained for sludges A and B after drying. In both cases, the isotherm corresponds to type IV in the BDDT classification. [20] The almost linear evolution observed at low pressure indicates that the system does not display any microporosity (pore diameter $d_p \leq 2$ *mn).* However, the hysteresis loop observed at high pressure shows that mesoporosity (2 nm< d_p< 50 nm) is present.

The corresponding total porous volumes (V_p), specific surfaces (S_{BET}), and BET constants (C_{BET}) are displayed in Table 3. These values reveal that both samples are porous, but develop a weak specific surface. Nevertheless, the comparison between isotherms obtained with the two sludge samples indicates that sludge A exhibits a more porous structure: it presents higher S_{BET} and V_p than sludge B. *t*-Plots (Fig. 3) confirm this analysis. In each case an upper deviation from the straight line is observed, which confirms that the structure is mainly mesoporous.[21] However, deviation is more important for sludge A, which indicates that mesoporosity is higher in this sludge than in sludge B.

Pore size distributions are calculated using the Broekhoff-de Boer method,[22] assuming that pores are open cylinders. Figure 4 shows that for both samples two close peaks are observed at about 3.5 and 5 nm. It also seems that both curves present a flatter peak between 25 and 30 nm. This last observation is further commented by analyzing mercury porosimetry experiments.

Table 2. *Initial mass, final mass, and water content of extruded samples of sludges A and B.*

	Sludge A		Sludge B	
	Extrudate 1	Extrudate 2	Extrudate 1	Extrudate 2
Initial mass (g)	1.953	1.959	1.978	1.899
Initial water content (kg/kg)	6.18	5.87	4.44	4.55
Final mass (g)	0.272	0.285	0.364	0.342

Table 3. *Total porous volumes (V_p), specific surfaces (S_{BET}), and BET constants (C_{BET}) for sludges A and B determined from N_2 adsorption-desorption isotherms.*

	V_P (cm^3/g)	S_{BET} (m^2/g)	C_{BET}
Sludge A	0.149	19	9.4
Sludge B	0.039	3.6	3.4

Figure 1. SEM images of external surface of sludge A (a: 50x, c: 5000x) and sludge B (b: 50x, d: 5000x).

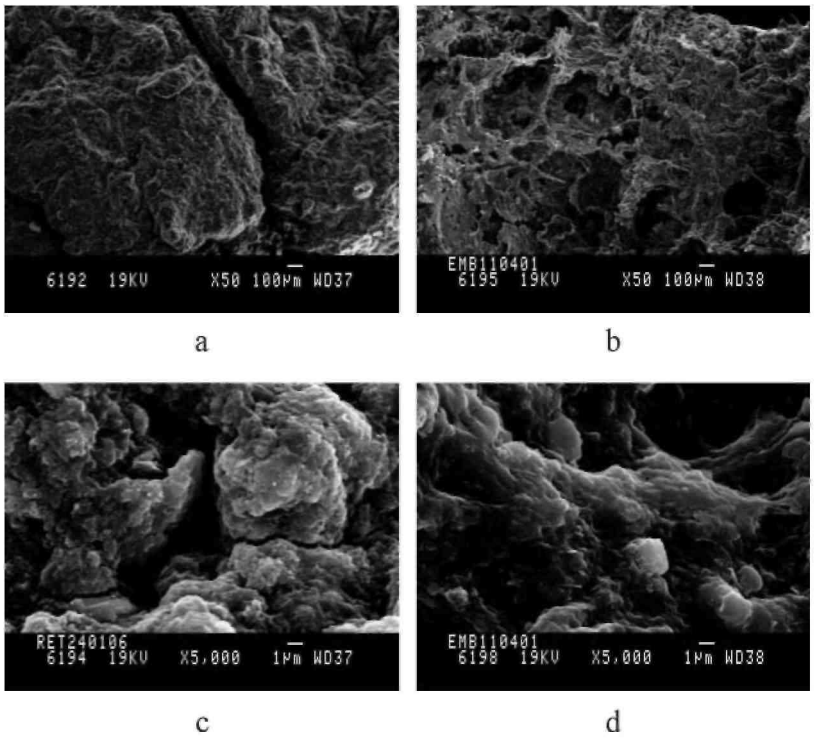

Figure 2. *Nitrogen adsorption and desorption curves of samples of sludges A and B.*

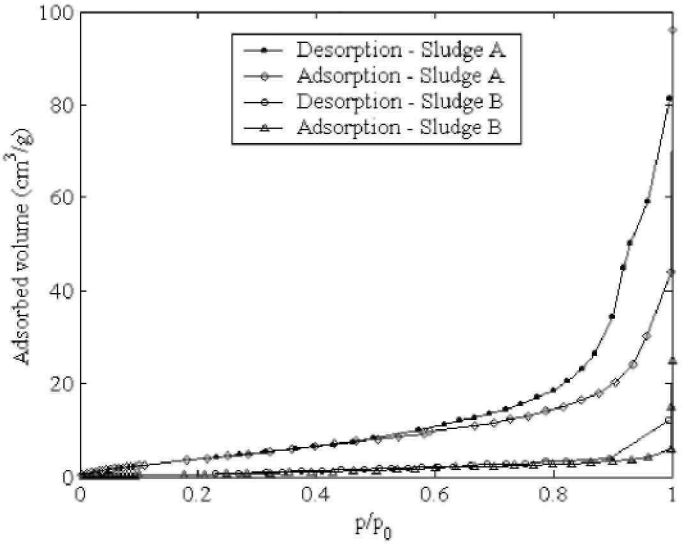

Figure 3. *t-Plots for samples of sludges A and B, based on N_2 sorption results.*

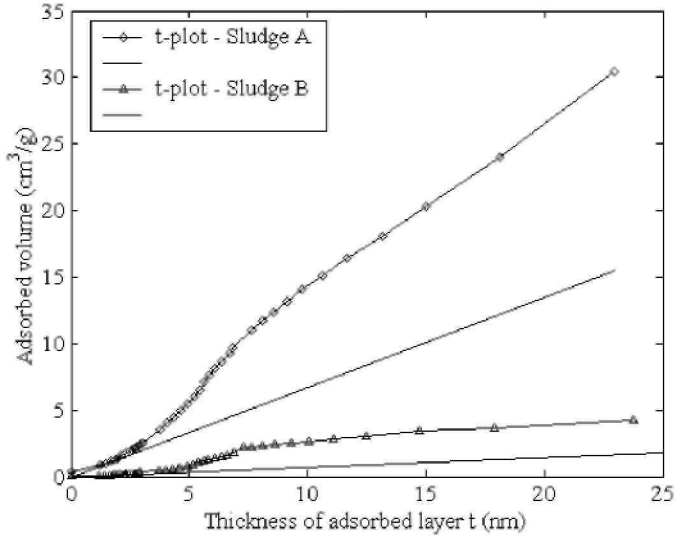

Mercury Porosimetry

Mercury porosimetry allows the investigation of pore diameter distribution in the range 7.5 nm-150 µm, i.e., overlapping the N_2 sorption range (0.5-50 nm). Figure 5 presents Hg porosimetry intrusion and extrusion curves. For sludge A mercury intrusion remains weak at low pressure (P < 1 MPa: $V_{Hg} \simeq 0.05$ cm^3/g). For higher pressures (P > 13 MPa), the sample is abruptly intruded by mercury. On the contrary, sludge B is gradually intruded by the mercury in the whole pressure range. The same behavior is observed for extrusion. In the case of sludge B, measurements between 90 and 200 MPa were hindered because of mechanical failure.

As samples are intruded without any collapse, the Washburn theory can be applied to determine the diameter of intruded pores (Eq. (1)).[23]

Figure 6 displays the evolution of cumulative pore volume vs. pore diameter in a semi-logarithmic plot. This graph shows different behaviors for sludges A and B. A kind of plateau is observed for sludge A, while the cumulative volume continuously increases with decreasing pore diameter for sludge B. As indicated in Table 4, the total porous volume V_{Hg} determined by mercury porosimetry in the range 16.6 nm < d_p < 95 µm is higher for sludge B than for sludge A. In the case of sludge B, 98% of V_{Hg} is formed by macropores (d_p > 50 nm) against 56% for sludge A. Table 4 also indicates that large pores investigated under atmospheric pressure (13 µm < d_p

<95µm) clearly contribute to the measured porous volume (35% of V_{Uq} for sludge A and 58% of V_{Hg} for sludge B).

Figure 7 shows the two pore volume distributions in a double-log plot. For both samples a small peak is detected around 16 µm, corresponding to pores investigated under atmospheric pressure. For sludge A, another peak at about 23 nm is clearly observed. This has to be related to the flat peak detected by N_2 sorption isotherms between 25 and 30 µm. Because of the mechanical failure that occurred during measurement on sludge B, the distribution is truncated on the left and no conclusion can be made.

As indicated by N_2 sorption curves and Hg porosimetry, sludges A and B present both mesopores and macropores. All pore diameters between 3 nm and 95 µm are represented with some predominant diameters: 3.5-5 nm and 25-30 nm in the mesoporous range and 16 µm in the macroporous range. Few data are available in the literature with which to compare our results. Couturier et al.[24] use mercury porosimetry (only above atmospheric pressure) and find that most of the pores in an activated sludge have a diameter inferior to 20 nm after drying. This result is close to those presented here, according to the diameter range investigated.

Figure 4. *Broekhoff-de Boer pore volume distribution for samples of sludges A and B, assuming that pores are open cylinders.*

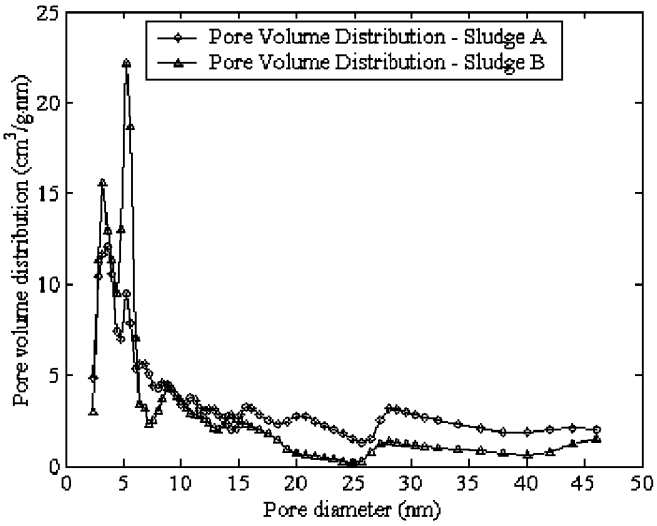

Figure 5. *Mercury intrusion and extrusion curves for samples of sludges A and B.*

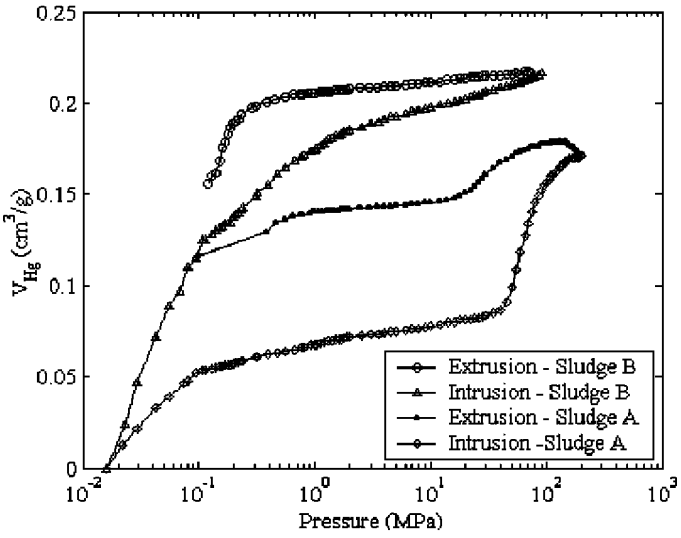

Figure 6. *Evolution of cumulated pore volume vs. pore diameter for sludges A and B.*

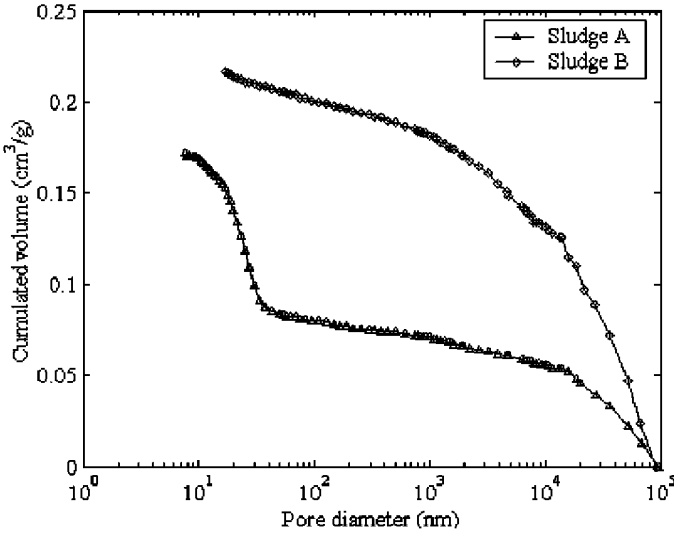

Table 4. *Analysis of cumulative pore volume curves determined by mercury porosimetry.*

	Total V_{Hg} 16.6 nm< d_p<95 μm (cm^3/g)	V_1 (cm^3/g)	V_2 (cm^3/g)
Sludge A	0.153	0.084 (56% of total V_{Hg})	0.054 (35% of total V_{Hg})
Sludge B	0.217	0.206 (95% of total V_{Hg})	0.126 (58% of total V_{Hg})

Note: V_1 is the volume corresponding to macropores, i.e., for d_p > 50 nm; V_2 is the volume corresponding to pores investigated under atmospheric pressure, i.e., for pore diameters in the range 13 µm <d_p<95 µm.

Figure 7. *Pore volume distribution from mercury porosimetry for samples of sludges A and B, in a double-log plot.*

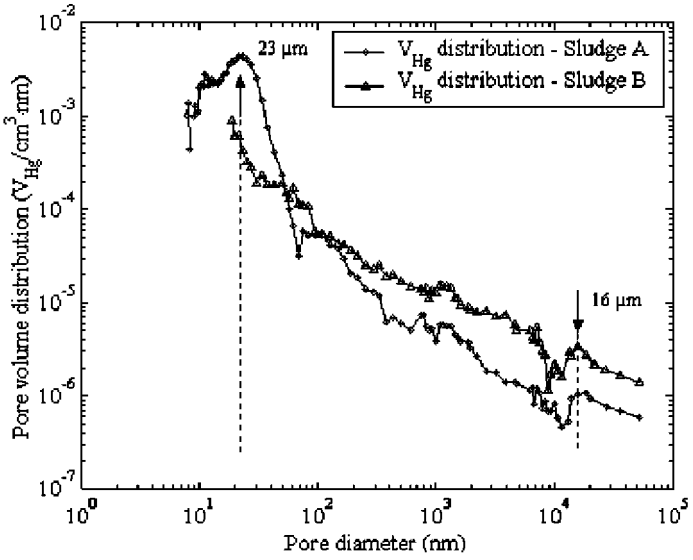

Microtomography

Microtomography allows the analysis of the material texture at a higher scale than SEM, N_2 isotherms analysis or mercury porosimetry: between the device spatial resolution of 41 µm and the maximal object size of about 20 mm. Table 5 displays initial (before drying) and final (after drying) equivalent diameters (Eq. (2)) and heights of the samples obtained by image analysis of tomographic images. It can be observed that all samples have initial

equivalent diameters greater than the die diameter (12 mm). This is an illustration of the swelling phenomenon that occurs during extrusion of viscoelastic materials.[25] Comparing the final dimensions of the two samples, one can observe that shrinkage is more important for sludge A than for sludge B. This is illustrated in Fig. 8 (shrinkage curves), which represents the evolution of the normalized sample volume V/V_0 vs. the normalized water content W/W_0. As explained in the material and methods section, there are two experimental points for each sludge at initial and final values of W/W_0, i.e., 0 and 1. Sludge A exhibits a higher shrinkage than sludge B, with a volume reduction of 80% against 60%. The volume decrease of both samples follows approximately the same trends till a normalized water content W/W_0 of approx. 0.5. Below this value, the two trends differ slightly. The volume decrease of sludge A remains linear, while shrinkage of sludge B slows down. Previous work shows that shrinkage of sludge A stops for water content near 0.2 kg/kg.[26] This is not observed on this figure, probably because the number of tomograms is not sufficient in the range of small water contents.

$$d = 2 \times \sqrt{\frac{\text{section area}}{\pi}} \qquad (2)$$

Figure 9 present cross-section images of the two samples at totally wet (a and b) and dry levels (c and d), i.e., respectively for W/W_Q equals to 1 and 0. Cross-sections of completely wet samples are rather similar, although sludge B (Fig. 9b) contains more voids and seems to have an initial diameter slightly larger than sludge A (as indicated by Table 5). When samples are completely dry, clear differences appear in the configuration of the cracks that developed during drying. Sludge A shows numerous cracks which are radially oriented, whereas for sludge B all solids are concentrated in an external crust delimiting a big internal void.

Table 5. *Initial and final equivalent diameters, initial and final heights for extruded samples of sludges A and B obtained from microtomographic investigation.*

	Sludge A		Sludge B	
	Extrudate 1	Extrudate 2	Extrudate 1	Extrudate 2
Initial equivalent diameter (mm)	12.74 ± 0.18	12.64 ± 0.08	13.00 ± 0.32	13.11 ± 0.12
Final equivalent diameter (mm)	7.40 ± 0.44	7.48 ± 0.39	10.09 ± 0.23	9.35 ± 0.90
Initial height (mm)	15.98 ± 0.34	15.91 ± 0.33	16.29 ± 0.29	16.36 ± 0.28
Final height (mm)	9.29 ± 0.20	9.04 ± 0.40	12.67 ± 0.10	12.67 ± 0.07

Figure 8. *Shrinkage curves. The points at $W/W_0=1$ and $W/W_0 = 0$ are slightly shifted to avoid superposition.*

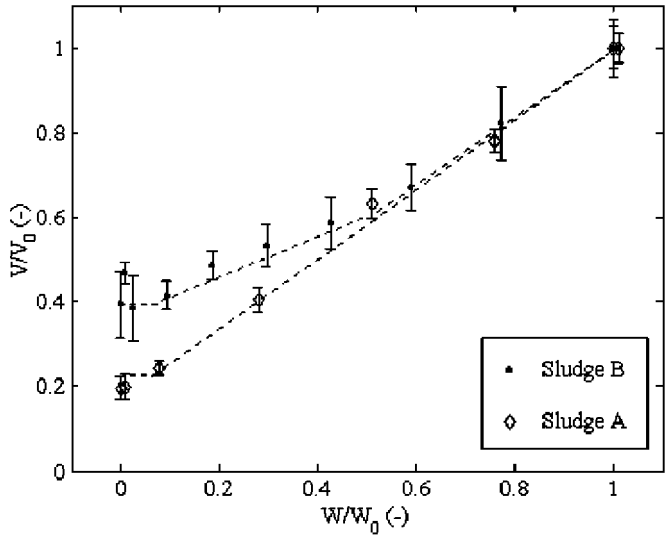

Figure 10 displays the development and extent of cracks at different drying levels: the "crack ratio" is defined as the area of cracks divided by the total area of the cross-section (including cracks and solid). The area of cracks and the total area of the section are obtained from the reconstructed 2D X-ray images. Discrimination among solid and void (cracks) regions within a cross section is achieved by binarization following Otsu's method.[27] Nonsignificant tiny objects (smallest than 3 by 3 pixels or, approximately, 0.015 mm^2) are removed by erosion. The final binary image is obtained by reconstruction of the thresholded image using the eroded image as marker. The crack area is calculated directly on the binarized image by multiplying the number of pixels constituting the cracks by a calibration constant. A closing operation is applied to reconstitute the external perimeter and to fill the image before calculating its total area. It can be seen on Fig. 10 that the crack ratio remains almost constant and quite low at high normalized water contents W/W_0, i.e., above 0.6 for sludge B and 0.4 to 0.3 for sludge A. Below these values, it starts to strongly increase indicating the onset of crack development. The final crack ratio is higher for sludge B than for sludge A, i.e., 60% vs. 40%. This difference is clearly illustrated on Figs. 9c and d. In a previous work, we showed that the expansion of cracks may be related to the development of internal transfer limitations.[28,29] The development of moisture gradients during the course of drying was clearly visualized by a grey level analysis of X-ray microtomograms. These moisture gradients, induced by the development of internal diffusional limitations, cause mechanical stresses leading to crack formation.[30,31]

It would be interesting to compare microtomography ($d_p > 41$ µm) results with those obtained with mercury porosimetry under atmospheric pressure (13 µm $< d_p <$ 95 µm). However the narrow overlapping range between these two techniques (41-95 µm) could induce large errors.

Figure 9. *Tomographic images of cross sections of sludge A (a: wet, c: dry) and sludge B (b: wet, d: dry).*

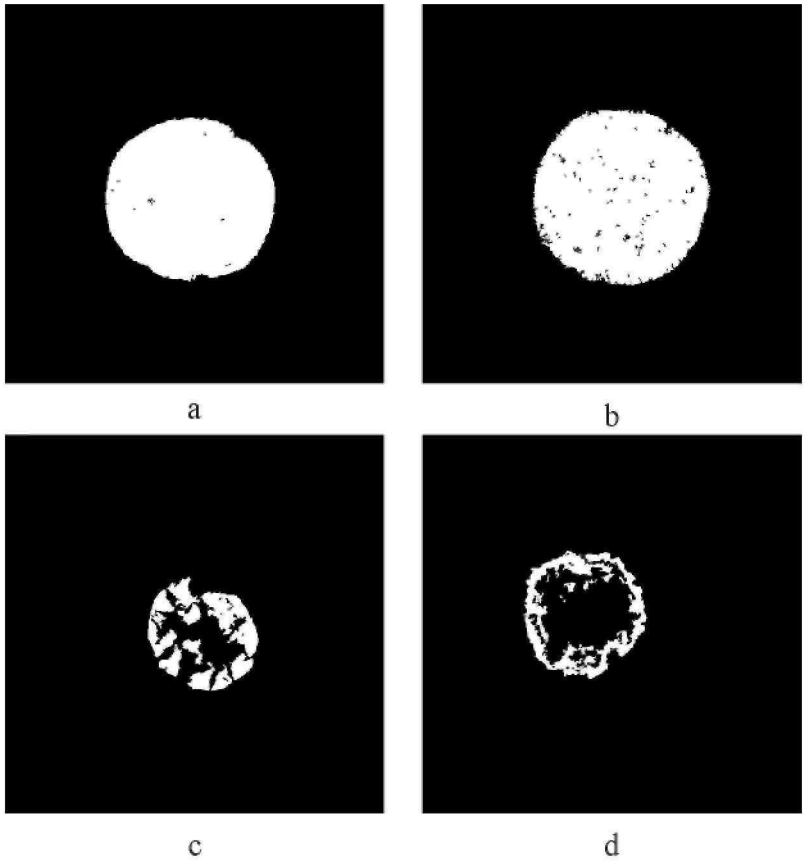

Figure 10. *Evolution of crack ratio measured by microtomography with normalized water content.*

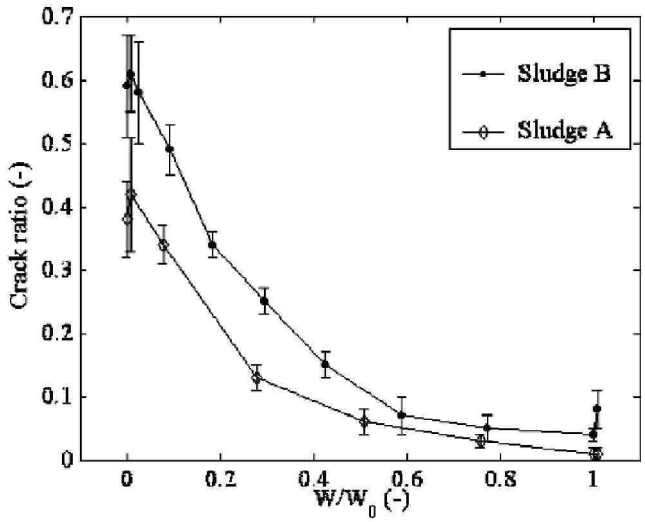

CONCLUDING REMARKS

In this work, two different wastewater sludges, conditioned, dewa-tered, and dried with the same operating conditions are characterized at several scales with independent techniques. N_2 isotherms and mercury porosimetry reveal a mesoporous and macroporous structure and indicate that the two sludges have low specific surfaces. These measurements also show that the porous volume and specific surface area are higher for sludge A. X-ray microtomography reveals different shrinkage behaviors of the two sludges, with a volume reduction of 80% for sludge A and 60% for sludge B. Microtomography appears to be an efficient technique to study the "ultramacroporosity" of the sludge samples and characterize their development during drying. Voids larger than 41 µm up to 2 cm can be detected and characterized. Results show that some cracks appear during drying. Their extent depends on the sludge: final crack ratio of 40% and 60% are reached respectively for sludge A and sludge B.

This work shows that each sludge has its own drying behavior. To our knowledge, this is the first time that the combination of these methods has been used to characterize this kind of material.

An interesting perspective would be to classify sludges on the basis of their composition and/or WTTP process characteristics in order to determine relations with their drying behavior. This is a big job, which will require confrontation of data acquired by different researchers involved in sludge drying, sludge dewatering, and wastewater treatment.

Nomenclature

C_{BET}	BET constant (—)
d	Equivalent diameter (mm)
d_p	Pore diameter (nm)
P	Pressure (MPa)
S_{BET}	BET specific surface area (m^2g^{-1})
V	Volume (m^3)
V_0	Initial volume (m^3)
V_1	Volume determined by mercury porosimetry corresponding to macropores (d_p > 50 nm) (m^3)

V_2 The volume determined by mercury porosimetry corresponding to pore investigated under atmospheric pressure (13 µm $< d_p <$ 95 µm) (m^3)

V_{Hg} Intruded mercury volume by mass unit (cm^3g^{-1})

V_p Porous volume determined at saturation pressure by N_2-isotherm analysis (cm^3g^{-1})

W Dry basis water content ($kg_{water}kg^{-1}Ds$)

W_0 Initial dry basis water content (kg_{water} $kg^{-1}DS$)

Greek Symbols

σ Surface tension of mercury ($N\ m^{-1}$)

θ Contact angle of mercury onto the pore walls (°)

Acronyms

DS Dry solid content

EU European union

WWTP Wastewater treatment plant

Acknowledgments

A. Léonard is grateful to the FNRS (National Fund for Scientific Research, Belgium) for a Ph.D. Research Fellow position. The Ministère de la Région Wallonne, the Ministère de la Communauté Française de Belgique, and the FNRS are also gratefully acknowledged for financial support.

References

1. Conseil de l'Union Européenne. Directive 1991/271/EC du 21 mai 1991 du Conseil relative au traitement des eaux urbaines résiduaires. OJ L 135 30.05.1991, 1991.

2. Conseil de l'Union Européenne. Directive 1999/31/EC du 26 avril 1999 du Conseil relative à la mise en décharge des déchets. OJ L 182 16.07.1999, 1999.

3. Hassebrauck, M.; Ermel, G. Two examples of thermal drying of sewage sludge. Wat. Sc. Tech. 1996, *33* (12), 235-242.

4. Kazakura, T.; Hasatani, M. R&D needs—drying of sludges. Drying Technol. 1996, *14* (6), 1389-1401.

5. Numrich, R.; Brown, B.W. Sludge drying with mechanical vapor re-compression. UTA International 1997, 2, 126-130.

6. Carrère-Gée, C; Lecomte, D.; Fudym, O.; Ledevie, B.; Vasseur, J. Determination of heat flux in thin layer drying of sludges. *Drying'98,* Proceedings of the 11th International Drying Symposium (IDS'98), Thessaloniki, Greece, Aug 19-22, 1998; Akritidis, C.B., Marinos-Kouris, D., Saravacos, G.D., Eds.; 1998; 695-702.

7. Léonard, A.; Crine, M. *Relation Between Convective Drying Kinetics and Shrinkage of Wastewater Treatment Sludges,* Proceedings of the 12th International Drying Symposium, Noordwijkerhout, The Netherlands, Aug 28-31, 2000; Kerkhof, P.J.A.M., Coumans, W.J., Mooiweer, G.D., Eds.; Elsevier Science B.V.: Amsterdam, 2000; Paper no. 131.

8. Vaxelaire, J.; Bongiovanni, J.-M.; Mousques, P.; Puiggali, J.R. Thermal drying of residual sludge. Wat. Res. 2000, *34* (17), 4318-4323.

9. Ferrasse, J.-H.; Arlabosse, P.; Lecomte, D. Heat, momentum, and mass transfer measurements in indirect agitated sludge dryer. Drying Technol. 2002, *20* (4 & 5), 749-769.

10. Léonard, A.; Blacher, S.; Marchot, P.; Crine, M. Use of X-ray microtomography to follow the convective heat drying of wastewater sludges. Drying Technol. 2002, *20* (4 & 5), 1053-1069.

11. Vaxelaire, J.; Puiggali, J.R. Analysis of the drying of residual sludge: from the experiment to the simulation of a belt dryer. Drying Technol. 2002, *20* (4 & 5), 989-1008.

12. Li, D.H.; Ganczarczyk, J.J. Structure of activated sludge flocs. Biotechnol. Bioengng. 1990, 35(1), 57-65.

13. Urbain, V.; Manem, J.; Block, J.C. Bioflocculation in activated sludge: an analytic approach. Wat. Res. 1993, 27(5), 829-838.

14. AFNOR. Tests on sludges—determination of properties related to thickening capacity. AFNOR T 97-001, 1979.

15. Serra, J. *Image Analysis and Mathematical Morphology;* Academic Press: New York, 1982; Vol. 1.

16. Coster, M.; Chermant, J.L. *Précis D'Analyse D'Images;* CNRS: Paris, 1985.

17. Léonard, A.; Blacher, S.; Marchot, P.; Pirard, J.P.; Crine, M. Image analysis of X-ray microtomograms of soft materials during convective drying. J. Microsc. (in press).

18. Washburn, E.W. Note on a method of determining the distribution of pore sizes in a porous material. Proc. Nat. Acad. Sci. 1921, 115.

19. Bierck, B.R.; Dick, R.I. Mechanisms of compressible sludge cake shrinkage. J. Environ. Eng.—ASCE 1990, *116* (4), 663-682.

20. Brunauer, S.; Deming, L.S.; Deming, W.S.; Teller, E. On a theory of the Van der Walls adsorption of gases. J. Am. Chem. Soc. 1940, *62*, 1723-1732.

21. Lecloux, A.J.; Pirard, J.P. The importance of standard isotherms in the analysis of adsorption isotherms for determining the porous structure of solids. J. Colloid Interface Sci. 1979, 70(2), 265-281.

22. Broekhoff, J.C.P.; de Boer, J.H. Studies on pore systems in catalysts, IX. Calculation of pore distributions from the adsorption branch of nitrogen sorption isotherms in the case of open cylindrical pores. J. Catal. 1967, 9(1), 8-14.

23. Alié, C; Pirard, R.; Pirard, J.P. Mercury porosimetry: applicability of the buckling-intrusion mechanism to low-density xerogels. J. Noncryst. Solids 2001, *292* (1-3), 138-149.

24. Couturier, S.; Vaxelaire, J.; Puiggali, J.R. *Convective Drying of Domestic Activated Sludge,* Proceedings of the 12th International Drying Symposium, Noordwijkerhout, The Netherlands, Aug 28-31, 2000; Kerkhof, P.J.A.M., Coumans, W.J., Mooiweer, G.D., Eds.; Elsevier: Amsterdam, 2000; Paper no. 44.

25. Boger, D.V.; Walters, K. *Rheological Phenomena in Focus;* Elsevier: Amsterdam, 1993.

26. Léonard, A.; Blacher, S.; Marchot, P.; Crine, M. *X-ray Microtomography: A New Tool to Follow Soft Material Shrinkage During Convective Drying,* Proceedings of the Second World Congress on Industrial Process Tomography, Hannover, Germany, Aug 29-31, 2001; 110-117.

27. Otsu, N. A threshold selection method from gray-level histograms. IEEE Trans. Syst. Man Cybern. 1979, *9* (1), 62-66.

28. Léonard, A. Etude du Séchage Convectif de Boues de Station D'épuration—Suivi de la Texture par Microtomographie à Rayons X. Ph.D. thesis, Université de Liège, Belgique, 2003.

29. Léonard, A.; Blacher, S.; Marchot, P.; Pirard, J.P.; Crine, M. Measurement of shrinkage and cracks associated to convective drying of soft materials by X-ray microtomography. Submitted to *Drying Technology.*

30. Liu, H.; Zhou, L.; Hayakawa, K.I. Sensitivity analysis for hygro-stress crack formation in cylindrical food during drying. J. Food Sci. 1997, *62* (3), 447-450.

31. Kim, J.-K.; Lee, C.-S. Prediction of differential drying shrinkage in concrete. Cement Concrete Res. 1998, *28* (7), 985-994.